FEBS Letters

FEBS PRESS science publishing by scientists

RESEARCH LETTER

Sticholysin I–II oligomerization in the absence of membranes

Sara García-Linares[1], Rafael Amigot-Sánchez[1], Carmen García-Montoya[1], Diego Heras-Márquez[1], Carlos Alfonso[2], Juan Román Luque-Ortega[3], José G. Gavilanes[1], Álvaro Martínez-del-Pozo[1] and Juan Palacios-Ortega[1,4]

1 Departamento de Bioquímica y Biología Molecular, Universidad Complutense, Madrid, Spain
2 Systems Biochemistry of Bacterial Division Lab, Centro de Investigaciones Biológicas Margarita Salas (CSIC), Madrid, Spain
3 Molecular Interactions Facility, Centro de Investigaciones Biológicas Margarita Salas (CSIC), Madrid, Spain
4 Biochemistry, Faculty of Science and Engineering, Åbo Akademi University, Turku, Finland

Correspondence
J. Palacios-Ortega, Departamento de Bioquímica y Biología Molecular, Universidad Complutense, Madrid, Spain
Tel: +34913944259
E-mail: juan.palaciosb1a@gmail.com

(Received 27 January 2022, revised 17 February 2022, accepted 24 February 2022, available online 9 March 2022)

doi:10.1002/1873-3468.14326

Edited by Maurice Montal

Sticholysins are pore-forming toxins produced by the sea anemone *Stichodactyla helianthus*. When they encounter a sphingomyelin-containing membrane, these proteins bind to it and oligomerize, a process that ends in pore formation. Mounting evidence indicates that StnII can favour the activity of StnI. Previous results have shown that these two isotoxins can oligomerize together. Furthermore, StnII appeared to potentiate the activity of StnI through the membrane-binding step of the process. Hence, isotoxin interaction should occur prior to membrane encounter. Here, we have used analytical ultracentrifugation to investigate the oligomerization of Stns in solution, both separately and together. Our results indicate that while StnI seems to be more prone to oligomerize in water solution than StnII, a small percentage of StnII in StnI–StnII mixtures promotes oligomerization.

Keywords: actinoporins; analytical ultracentrifugation; pore-forming proteins; sedimentation velocity

Actinoporins are pore-forming toxins found in the venom of many species of sea anemones [1–3]. The most studied actinoporins are sticholysins (Stns), produced by *Stichodactyla helianthus* [4–6], equinatoxins, from *Actinia equina* [7,8], and fragaceatoxins, from *Actinia fragacea* [9–11]. The sequences of actinoporins are usually very similar, sharing in most cases > 60% sequence identity [3,12,13]. This is especially remarkable in the case of isotoxins because many sea anemones, including the ones listed above, produced these isotoxins simultaneously [1,2,10,14–16]. The variation of the amino acid sequence among isotoxins from the same sea anemone species is much smaller than the average value obtained when considering other actinoporins. For example, StnI and StnII present a ~ 93% sequence identity (~ 94% similarity), EqtII and EqtIV, an ~ 87% (~ 94% similarity), and FraC and FraE, a ~ 98% (all but two residues).

It is striking that these small differences have, most often, a great impact on the activity of each of these proteins when assayed against both model membranes and erythrocytes [17]. These functional disparities have given rise to a variety of hypotheses regarding the existence of actinoporin isotoxins within single sea anemone individuals. One of the most popular is that this diversity could help broaden the range of accessible targets, both offensively and defensively [18–20]. Accordingly, one could expect the isotoxins to act separately. However, they are co-purified when the sea anemones are used directly as the toxin source [8,21–

Abbreviations
DLS, dynamic light scattering; Eqt, equinatoxin; Stn, sticholysin.

23]. Taking this into account, it is feasible to speculate if some combined action between them may occur during the process of pore formation. Independent recombinant expression of the individual isotoxins allows to approach this question without interference of cross-contamination.

This is precisely what was observed for sticholysins [18]. A given concentration of a StnI–StnII mixture was shown to produce an effect not only greater than that of the same concentration of StnI alone, but also greater than that sum of the effect of the corresponding fractional concentrations of StnI and StnII present in those samples. Results of that study [18] also indicated that the interaction between the isotoxins took place, at least, during the membrane-binding steps of the pore-formation process. Hence, oligomerization in solution could be expected. In fact, StnII is known to form dimeric and tetrameric ensembles in absence of membranes [24]. In a much recent study [25], we also detected oligomerization of StnI and StnI–StnII mixtures in solution. However, the signal was very small, preventing the determination and quantification of the different oligomeric species.

To delve deeper into this phenomenon, we have now turned to analytical ultracentrifugation, using sedimentation velocity experiments, a hydrodynamic method that allows the determination of size, shape and interactions of the studied molecules [26–29]. Dynamic light scattering (DLS) was used to measure the Stokes radii of the monomeric species of StnI and StnII. Our results indicate that, separately, StnI is more prone to oligomerize than StnII. However, small amounts of StnII can increase the fraction of oligomeric species in StnI–StnII mixtures, in accordance with our previous activity results.

Materials and methods

Recombinant StnI and StnII were produced in *Escherichia coli*, strand RB791, and purified to homogeneity as described in Ref. [30]. Sedimentation velocity experiments were performed at 48 000 rpm (170 000 ***g***) in an XL-I analytical ultracentrifuge (Beckman-Coulter Inc., Brea, CA, USA) equipped with both UV–VIS absorbance and Raleigh interference detection systems, using an An-50Ti rotor (Beckman-Coulter Inc.) at 20 °C. Samples in 15 mM MOPS, 100 mM NaCl buffer, pH 7.5, were loaded (320 µL) into 12-mm Epon-charcoal standard double-sector centerpieces, except for highly concentrated samples, where 3-mm centerpieces were used. The partial specific volume was calculated from the amino acid sequences by SEDNTERP [31], being 0.7324 and 0.7338 $mL{\cdot}g^{-1}$ for StnI and StnII respectively. This allows to approximate the M_w.

Concentration scans were performed for both isotoxins separately, beginning at ~ 6 µM, and ending at ~ 390 µM. Sedimentation was followed using both interference and absorbance at 250 nm. At the highest concentration, interference data were used. StnI–StnII mixtures at various ratios were assayed at a total protein concentration of 150 µM. In this case, sedimentation was followed using absorbance at 300 nm. Differential sedimentation coefficient distributions were calculated by least-squares boundary modelling of sedimentation velocity data using the continuous distribution c(*s*) Lamm equation model as implemented by SEDFIT [32]. These experimental s values were corrected to standard conditions using the program SEDNTERP [31] to get the corresponding standard s values ($s_{20,w}$).

For the separate isotoxins, it was possible to use the weight-averaged sedimentation coefficients results to fit the following isotherm

$$s_w(c_{tot}) = \sum_i \frac{s_{0,i}}{1 + k_{s,i}K_i c_1^i} \frac{K_i c_1^i}{c_{tot}} \cong \frac{1}{1 + k_s c_{tot}} \sum_i s_{0,i} \frac{K_i c_1^i}{c_{tot}}, \quad (1)$$

where $s_{0,i}$ is the species sedimentation coefficients, $k_{s,i}$ is their hydrodynamic nonideality coefficients, K_i is the association constants (with $K_1 = 1$), c_1^i is the concentration of monomers in the samples regardless of their oligomerization state and c_{tot} is the sum of the concentrations of all oligomeric species. In our case, we used the second part of Eqn (1), where the hydrodynamic nonideality coefficient is assumed to be the same for all species in the sample. In all cases, the value of the parameter was $< 5 \times 10^{-4}$, indicating that the systems behave ideally. The calculated M_w of the oligomers observed in the sedimentation coefficient distribution [c(*s*)] was used to estimate the stoichiometry of the oligomers. Accordingly, Eqn (1) was used so that it described a monomer–dimer–tetramer system [33,34].

The association constants obtained were used to calculate the oligomer fractions as function of total toxin concentration in the sample, which were compared to the fractions of each species calculated according to the *c*(*s*) obtained.

This approach was also used to study the formation of heteromers in the mixtures of StnI and StnII. However, no satisfactory fits were obtained in this case.

The buffer for DLS (same composition as above) was filtered through 0.2-µm filters. Final toxin concentrations were 16 and 8.3 µM of StnI and StnII respectively.

Results and Discussion

StnI

Results from the concentration scan using StnI revealed the existence, in most cases, of three peaks in the *c*(*s*) distribution, whose relative areas were

dependent on the loading concentration of StnI. Given that the peaks obtained are well clearly resolved from one another (Fig. 1A), the equilibrium between the oligomeric ensembles of StnI in solution does not seem to change much in the time scale of these experiments (~ 5.5 h) [27,28].

The values of $s_{w,20}$, and the approximates for M_w obtained from the analysis are presented in Table 1. The estimated M_w for the ensembles of the population with the smallest sedimentation coefficient was 24.6 ± 1.6 kDa, compatible with the M_w of StnI monomers (M_w = 19 391 Da, according to the sequence). The upward deviation of the value is a consequence of the analysis and the significant population of larger oligomers detected which, during the fitting process, results in an average frictional coefficient that is overestimated for this population. The estimate for the Stokes radius (r_{Stokes}) of the monomers was 27.5 ± 2.0 Å. This value is an approximation and shows distortion from the analysis. The value obtained using DLS is 22.0 ± 4.5 Å. The latter value also agrees with the dimensions expected for a StnI monomer according to the available three-dimensional structures [35]. The estimated M_w of the second population was 44.4 ± 4.2 kDa, indicating that it was most likely composed of StnI dimers. This value is again larger than the theoretical value, but follows the deviation explained above. The last detectable population had an estimated M_w of 73.4 ± 4.3 kDa, compatible with that of a slightly elongated StnI tetramer.

The fact that no population compatible with the M_w of StnI trimers was detected suggests that the likeliest pathway to tetramers is the condensation of dimers, with monomer–dimer interactions thus being somehow less favourable. This could be consequence of some dimerization-induced conformational change that, affecting both monomers involved, would alter their structure just enough so that a dimer–dimer interaction would be more favourable in water solution than monomer–dimer associations. This could also contribute to trimer scarcity by reducing the population of monomers, which are required to form trimers.

The isotherm fit to the weight-averaged sedimentation coefficients (Fig. 2A) allowed to estimate the association constants of the oligomers, obtaining values of 3×10^3 M^{-1} and 2×10^{10} M^{-3} for the dimerization and tetramerization equilibria respectively. These constants were then used to calculate the fractional population of each oligomeric species as a function of StnI concentration (Fig. 2B).

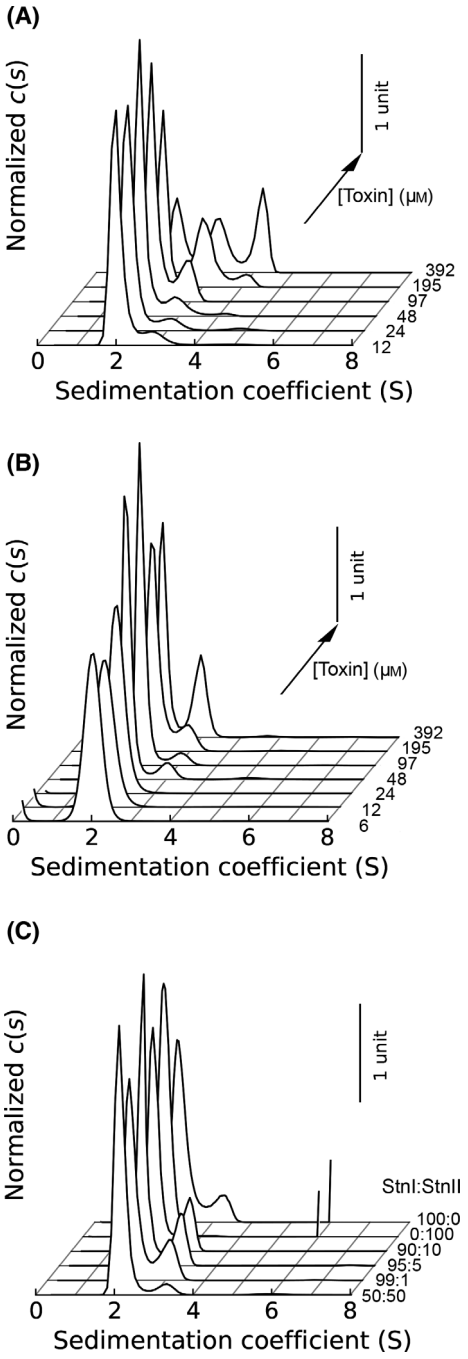

Fig. 1. Sedimentation coefficient distributions *c*(*s*) obtained from the analysis of the sedimentation profiles of the concentration scans performed with StnI (A), StnII (B) and the mixture of both (C). Toxin concentration (μM) used in each separate experiment is indicated on the right, except for (C) where StnI:StnII protein ratios are shown using a total protein concentration of 150 μM. The *c*(*s*) distributions were normalized so that the area beneath each curve was the same in all cases to facilitate comparison between experiments.

Table 1. Values of $s_{20,w}$ (S) derived from the sedimentation velocity experiments of StnI and StnII independently, and from those in which StnI–StnII mixtures were used. Values for M_w and stoichiometry are estimates from the analysis. In each case, except for StnI–StnII mixtures at 150 μM, three populations could be detected in some of the samples. The monomer M_w based on the sequence of StnI and StnII is 19 391 and 19 283 Da respectively. Indicated values are average ± SD of n = 2–6.

	$s_{20,w}$ (S)	M_w estimates (kDa)	Stoichiometry (x monomer M_w)
StnI	2.13 ± 0.04	24.6 ± 1.6	1.27 ± 0.09
	3.15 ± 0.09	44.4 ± 4.2	2.29 ± 0.22
	4.28 ± 0.07	73.4 ± 4.3	3.79 ± 0.22
StnII	2.13 ± 0.03	20.6 ± 0.8	1.07 ± 0.04
	3.11 ± 0.04	36.1 ± 2.4	1.86 ± 0.13
	5.37 ± 0.47	81.2 ± 12.5	4.19 ± 0.65
StnI + StnII	2.26 ± 0.04	17.7 ± 0.5	0.91 ± 0.02
	3.26 ± 0.14	31.4 ± 3.2	1.62 ± 0.17

StnII

When identical experiments were performed with StnII, the results also suggested that the oligomerization equilibrium between StnII's protomers in solution can also be considered static in the time scale of the assay (Fig. 1B). However, the analysis revealed some differences with StnI. First, only two major peaks were detected in most cases, with the second one becoming prominent only at the higher toxin concentrations. However, while in the case of StnI only three populations were required to adequately describe the sedimentation data, StnII showed residual populations (< 0.7% total) of higher sedimentation coefficients (> 6.5 S). These observations were more evident at the highest StnII concentration assayed (Fig. 3).

The values of $s_{w,20}$, and the approximates for M_w obtained from the sedimentation velocity analysis are presented in Table 1. The estimate for the Stokes radius (r_{Stokes}) of the monomers was 22.7 ± 0.8 Å, an identical value to the DLS result of 22.5 ± 4.5 Å (DLS results are the same for StnI and StnII). As for StnI, no peaks compatible with trimers were observed, again suggesting that the formation of tetramers would occur *via* dimer condensation.

Isotherm fitting was now performed with these results (Fig. 2C), yielding association constants of 2×10^3 M^{-1} and 3×10^9 M^{-3} for the dimerization and tetramerization respectively. These results are reassuring, since the monomer–tetramer association constant for StnII was already reported to be in the range of 10^9 M^{-3} [24]. As for StnI, the association constants

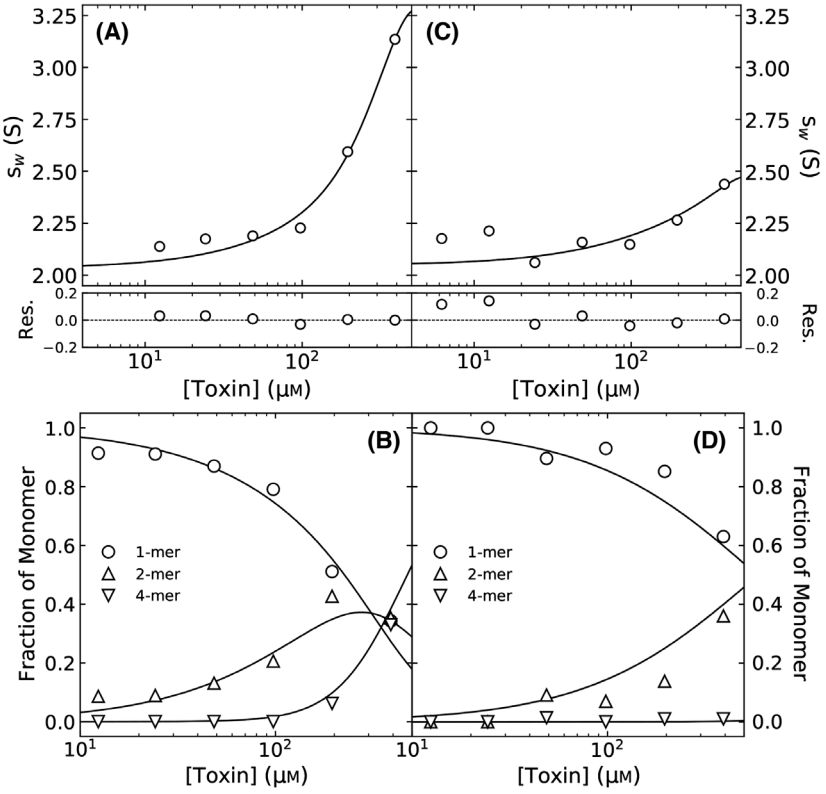

Fig. 2. (A) Isotherm of the weight-averaged sedimentation coefficient as a function of StnI concentration. The lower panel shows the residuals of the fitting. (B) Fraction of each detected StnI oligomeric species as a function of toxin concentration. Lines were drawn using the association constants obtained with the fitting shown in A. (C) Isotherm of the weight-averaged sedimentation coefficient as a function of StnII concentration. The lower panel shows the residuals of the fitting. (D) Fraction of each detected StnII oligomeric species as a function of toxin concentration. Lines were drawn using the association constants obtained with the fitting shown in C.

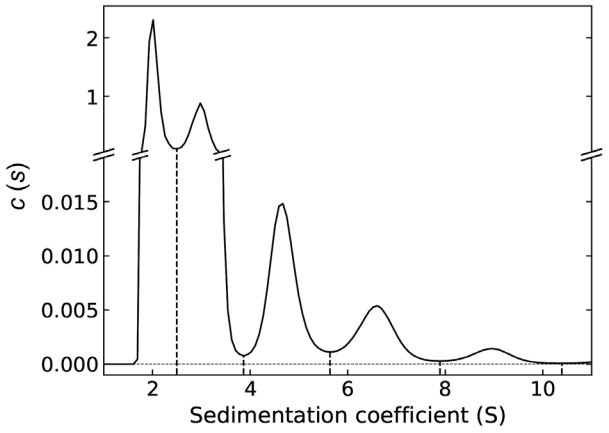

Fig. 3. Sedimentation coefficient distribution $c(s)$ obtained from the analysis of the assay with StnII at 392 μM. The lower part of the graph shows a magnification of the $c(s)$ distribution, allowing to resolve two more oligomer populations beyond the one corresponding to tetramers, which is centred at ~ 5 S. These two peaks represent only ~ 0.7% of the total. Their estimated M_w of 111 and 176 kDa, respectively, would correspond to hexameric and nonameric ensembles of StnII.

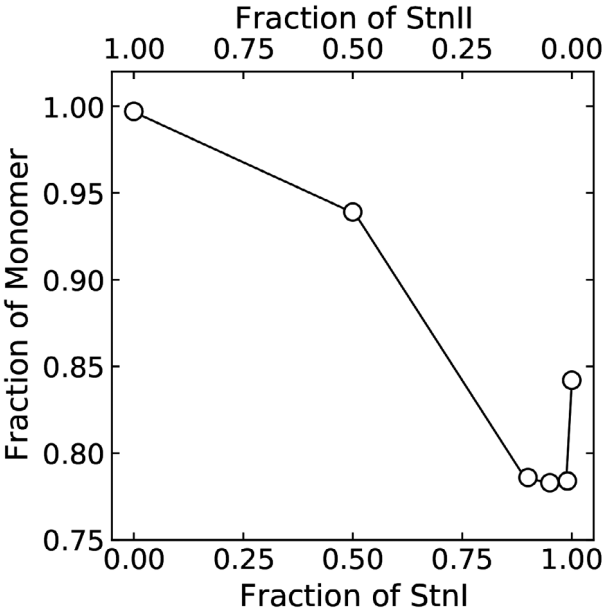

Fig. 4. Fraction of monomer as a function of the relative sample content of StnI and StnII. In most cases, only a population of dimers was detected. In case tetramers were also detected, they summed up to less than 1% of the total. Hence, only monomer fraction is displayed. Note that, for the conditions used in these experiments, small fractions of StnII (≤ 10%) induce a minimum in the monomer population compared to other sample compositions.

were used to calculate the fraction of each oligomeric species as a function of StnII concentration (Fig. 2D).

StnI–StnII mixtures

Sedimentation velocity experiments were next performed using StnI–StnII mixtures to see how their relative concentrations affected the oligomerization equilibrium in absence of membranes. These experiments were performed using total toxin concentration of 150 μM.

The values of $s_{w,20}$, and the approximates for M_w obtained for all detected oligomeric populations are shown in Table 1. As for StnI and StnII separately, the estimates for the M_w of most of the detected ensembles were consistent with those of monomers and dimers.

The fraction of monomers for all StnI–StnII mixtures assayed is shown in Fig. 4. It is interesting to notice that the fraction of monomers reaches a minimum, that is, a maximum in dimers, when the fraction of StnII is ≤ 10%, despite StnII been less prone to oligomerize than StnI. In those experiments, the effective StnI concentration has been reduced compared to when the fraction of StnI was 100%. For this reason, if the oligomerization equilibria were independent, the total monomer fraction in the sample should be increased, as the equilibria would be displaced towards monomers. However, this is not the case, indicating that hetero-oligomers are being formed. This observation would support the hypothesis that StnII, despite being less likely to oligomerize with itself, can promote the oligomerization of StnI [18]. In fact, possible residue interactions underlying this preference have already been proposed [25]. Based on FRET results using fluorescently labelled StnI, it was discussed how, apparently, StnII monomer–monomer associations would be more favourable than those of only StnI. Briefly, this would be so because, of the only 12 residues that differ between StnI and StnII, two of them are located on the monomer–monomer interface, according to the available pore structures of actinoporins [11]. The residue pairs that these amino acids would form with their complementary counterparts would stablish stronger interactions for StnII than for StnI. However, given that both differences are on the same side of the toxin, a StnI–StnII dimer in the appropriate order, though not on the contrary, would, in principle, preserve the interactions that are presumed to occur on a StnII dimer (Fig. 5). Given that the population of sticholysin trimers is not detectable (at least in absence of membranes), further suggest that StnII monomers would present a preference to interact with StnI monomers but only using the most favourable monomer–monomer interface of the two available possibilities.

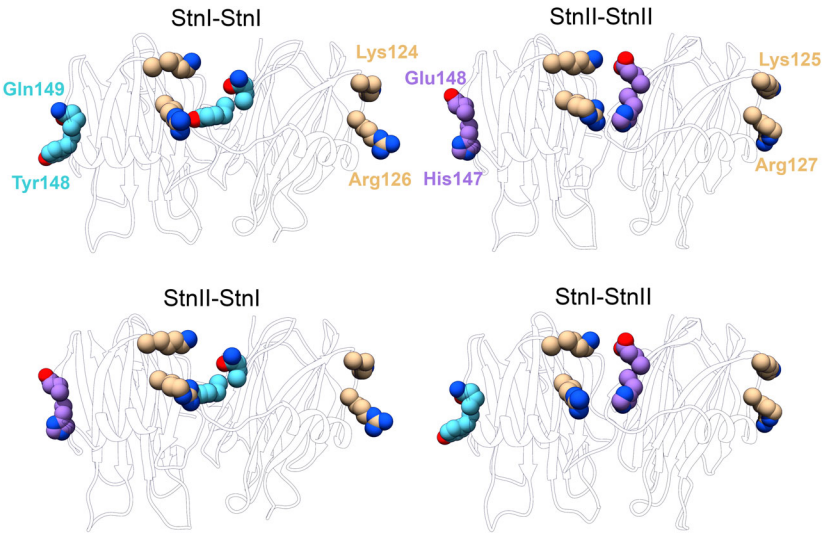

Fig. 5. Possible dimers formed by StnI, StnII and StnI with StnII. Side chain conformation is not necessarily representative of that occurring in the oligomers, as these structures (PDB access codes: 2KS4 for StnI and 1GWY for StnII) were obtained by X-ray crystallography and NMR. Notice that the monomer–monomer interfaces are the same on each column, regardless of the ensembles being homodimers or heterodimers.

The role of these soluble oligomers in the process of pore formation, regardless of their isotoxin composition, remains unclear. Recent results suggest that these ensembles could be better at sphingomyelin recognition in membranes that lack Chol [25]. It is also likely that they may act as protomers, speeding up toxin oligomerization once on the membrane surface. However, further experiments are required to solve these questions.

Conclusions

In this study, the oligomerization of StnI and StnII in absence of lipid membranes has been studied using analytical ultracentrifugation and DLS, in particular sedimentation velocity experiments. These experiments have allowed us to determine the association constants for dimerization and tetramerization for StnI and StnII in solution, revealing that StnI is more prone to form oligomers, especially tetramers, than StnII. Not only that, but we have also observed that StnII is able to promote dimer formation in StnI–StnII mixtures beyond the oligomerization observed for StnI at ratios in which StnII is the minority component. Finally, we have proposed a hypothesis that might explain this behaviour based on the structure of both toxins and their potential monomer–monomer interactions. The role played by these oligomers in the process of pore formation is still an open question in the field and will certainly be the subject of future studies.

Acknowledgements

This research was supported by the Juselius Foundation (JP-O), UCM-Banco Santander Grants PR75/18-21561 and PR87/19-22556, and UnaEuropa (Unano) SF2106 (to AM-d-P) and Spanish Ministry of Science and Innovation PID2019-104544GB-I00 (CA). JP-O has a funded doctoral student position from ISB/ÅA. JRL-O acknowledges support from the Molecular Interactions Facility funds at the CIB-CSIC.

Author contributions

SG-L, RA-S and CG-M prepared the samples for analysis. CA and JRL-O performed the ultracentrifugation experiments and the analysis to obtain the $c(s)$ distributions. DH-M and JP-O prepared the samples for DLS. JP-O prepared the figures, performed the oligomerization analysis and wrote the first draft of the manuscript. All authors revised the final version of the manuscript, providing comments and corrections.

Data accessibility

The data supporting the findings of this study are available from the corresponding author (juan.palaciosb1a@gmail.com) upon reasonable request.

References

1 Maček P. Polypeptide cytolytic toxins from sea anemones (Actiniaria). *FEMS Microbiol Immunol.* 1992;**5**:121–9.
2 Alegre-Cebollada J, Oñaderra M, Gavilanes JG, Martínez-del-Pozo A. Sea anemone actinoporins: the transition from a folded soluble state to a functionally active membrane-bound oligomeric pore. *Curr Protein Pept Sci.* 2007;**8**:558–72.
3 Palacios-Ortega J, García-Linares S, Rivera-de-Torre E, Heras-Márquez D, Gavilanes JG, Slotte JP, et al.

Structural foundations of sticholysin functionality. *Biochim Biohys Acta Proteins Proteom*. 2021;**1869**:140696.
4 Tejuca M, Dalla Serra M, Ferreras M, Lanio ME, Menestrina G. Mechanism of membrane permeabilization by sticholysin I, a cytolysin isolated from the venom of the sea anemone *Stichodactyla helianthus*. *Biochemistry*. 1996;**35**:14947–57.
5 De los Ríos V, Mancheño JM, Lanio ME, Oñaderra M, Gavilanes JG. Mechanism of the leakage induced on lipid model membranes by the hemolytic protein sticholysin II from the sea anemone *Stichodactyla helianthus*. *Eur J Biochem*. 1998;**252**:284–9.
6 Rivera-de-Torre E, Martínez-del-Pozo A, Garb JE. *Stichodactyla helianthus*' de novo transcriptome assembly: discovery of a new actinoporin isoform. *Toxicon*. 2018;**150**:105–14.
7 Ferlan I, Lebez D. Equinatoxin, a lethal protein from *Actinia equina*—I Purification and characterization. *Toxicon*. 1974;**12**:57–8.
8 Maček P, Lebez D. Isolation and characterization of three lethal and hemolytic toxins from the sea anemone *Actinia equina* L. *Toxicon*. 1988;**26**:441–51.
9 Mechaly AE, Bellomio A, Morante K, González-Mañas JM, Guerin DM. Crystallization and preliminary crystallographic analysis of fragaceatoxin C, a pore-forming toxin from the sea anemone *Actinia fragacea*. *Acta Crystallogr Sect F Struct Biol Cryst Commun*. 2009;**65**:357–60.
10 Bellomio A, Morante K, Barlič A, Gutiérrez-Aguirre I, Viguera AR, González-Mañas JM. Purification, cloning and characterization of fragaceatoxin C, a novel actinoporin from the sea anemone *Actinia fragacea*. *Toxicon*. 2009;**54**:869–80.
11 Tanaka K, Caaveiro JM, Morante K, González-Mañas JM, Tsumoto K. Structural basis for self-assembly of a cytolytic pore lined by protein and lipid. *Nat Commun*. 2015;**6**:1–11.
12 García-Ortega L, Alegre-Cebollada J, García-Linares S, Bruix M, Martínez-del-Pozo A, Gavilanes JG. The behavior of sea anemone actinoporins at the water-membrane interface. *Biochim Biophys Acta*. 2011;**1808**:2275–88.
13 García-Linares S, Rivera-de-Torre E, Palacios-Ortega J, Gavilanes JG, Martínez-del-Pozo A. The metamorphic transformation of a water-soluble monomeric protein into an oligomeric transmembrane pore. In: Iglič A, Rappolt M, García-Sáez AJ, editors. Advances in biomembranes and lipid self-assembly. Amsterdam: Elsevier; 2017. p. 51–97.
14 Monastyrnaya M, Leychenko E, Isaeva M, Likhatskaya G, Zelepuga E, Kostina E, et al. Actinoporins from the sea anemones, tropical *Radianthus macrodactylus* and northern *Oulactis orientalis*: comparative analysis of structure-function relationships. *Toxicon*. 2010;**56**:1299–314.
15 Khoo KS, Kam WK, Khoo HE, Gopalakrishnakone P, Chung MC. Purification and partial characterization of two cytolysins from a tropical sea anemone, *Heteractis magnifica*. *Toxicon*. 1993;**31**:1567–79.
16 Tkacheva E, Leychenko E, Monastyrnaya M, Issaeva M, Zelepuga E, Anastuk S, et al. New actinoporins from sea anemone *Heteractis crispa*: cloning and functional expression. *Biochemistry*. 2011;**76**:1131.
17 García-Linares S, Rivera-de-Torre E, Morante K, Tsumoto K, Caaveiro JM, Gavilanes JG, et al. Differential effect of membrane composition on the pore-forming ability of four different sea anemone actinoporins. *Biochemistry*. 2016;**55**:6630–41.
18 Rivera-de-Torre E, García-Linares S, Alegre-Cebollada J, Lacadena J, Gavilanes JG, Martínez-del-Pozo A. Synergistic action of actinoporin isoforms from the same sea anemone species assembled into functionally active heteropores. *J Biol Chem*. 2016;**291**:14109–19.
19 Basulto A, Pérez VM, Noa Y, Varela C, Otero AJ, Pico MC. Immunohistochemical targeting of sea anemone cytolysins on tentacles, mesenteric filaments and isolated nematocysts of *Stichodactyla helianthus*. *J Exp Zoolog A Comp Exp Biol*. 2006;**305**:253–8.
20 Wang Y, Yap LL, Chua KL, Khoo HE. A multigene family of *Heteractis* magnificalysins (HMgs). *Toxicon*. 2008;**51**:1374–82.
21 Kem WR, Dunn BM. Separation and characterization of four different amino acid sequence variants of a sea anemone (*Stichodactyla helianthus*) protein cytolysin. *Toxicon*. 1988;**26**:997–1008.
22 Lanio ME, Morera V, Álvarez C, Tejuca M, Gómez T, Pazos F, et al. Purification and characterization of two hemolysins from *Stichodactyla helianthus*. *Toxicon*. 2001;**39**:187–94.
23 Morante K, Bellomio A, Viguera AR, Gonzalez-Manas JM, Tsumoto K, Caaveiro JMM. The isolation of new pore-forming toxins from the sea anemone *Actinia fragacea* provides insights into the mechanisms of actinoporin evolution. *Toxins (Basel)*. 2019;**11**:401.
24 De los Ríos V, Mancheño JM, Martínez-del-Pozo A, Alfonso C, Rivas G, Oñaderra M, et al. Sticholysin II, a cytolysin from the sea anemone *Stichodactyla helianthus*, is a monomer-tetramer associating protein. *FEBS Lett*. 1999;**455**:27–30.
25 Palacios-Ortega J, Rivera-de-Torre E, García-Linares S, Gavilanes JG, Martínez-del-Pozo Á, Slotte JP. Oligomerization of sticholysins from Förster resonance energy transfer. *Biochemistry*. 2021;**60**:314–23.
26 Laue TM, Stafford WF III. Modern applications of analytical ultracentrifugation. *Annu Rev Biophys Biomol Struct*. 1999;**28**:75–100.
27 Lebowitz J, Lewis MS, Schuck P. Modern analytical ultracentrifugation in protein science: a tutorial review. *Protein Sci*. 2002;**11**:2067–79.

28 Howlett GJ, Minton AP, Rivas G. Analytical ultracentrifugation for the study of protein association and assembly. *Curr Opin Chem Biol*. 2006;**10**:430–6.
29 Cole JL, Lary JW, Moody TP, Laue TM. Analytical ultracentrifugation: sedimentation velocity and sedimentation equilibrium. *Methods Cell Biol*. 2008;**84**:143–79.
30 Alegre-Cebollada J, Clementi G, Cunietti M, Porres C, Oñaderra M, Gavilanes JG, et al. Silent mutations at the 5'-end of the cDNA of actinoporins from the sea anemone *Stichodactyla helianthus* allow their heterologous overproduction in *Escherichia coli*. *J Biotechnol*. 2007;**127**:211–21.
31 Laue T, Shah B, Ridgeway T, Pelletier S. Computer-aided interpretation of analytical sedimentation data for proteins. In: Harding SE, Rowe AJ, Horton JC, editors. Analytical ultracentrifugation in biochemistry and polymer science. Cambridge: Royal Society of Chemistry; 1992. p. 90–125.
32 Schuck P. Size-distribution analysis of macromolecules by sedimentation velocity ultracentrifugation and Lamm equation modeling. *Biophys J*. 2000;**78**:1606–19.
33 Schuck P. On the analysis of protein self-association by sedimentation velocity analytical ultracentrifugation. *Anal Biochem*. 2003;**320**:104–24.
34 Frigon RP, Timasheff SN. Magnesium-induced self-association of calf brain tubulin. I. Stoichiometry. *Biochemistry*. 1975;**14**:4559–66.
35 García-Linares S, Castrillo I, Bruix M, Menéndez M, Alegre-Cebollada J, Martínez-del-Pozo A, et al. Three-dimensional structure of the actinoporin sticholysin I. Influence of long-distance effects on protein function. *Arch Biochem Biophys*. 2013;**532**:39–45.